Int J Fract
DOI 10.1007/s10704-009-9426-4

ORIGINAL PAPER

Supersonic cracks in lattice models

T. M. Guozden · E. A. Jagla · M. Marder

Received: 2 December 2008 / Accepted: 2 November 2009

Abstract We have studied cracks traveling along weak interfaces. We model them using harmonic and anharmonic forces between particles in a lattice, both in tension (Mode I) and antiplane shear (Mode III). One of our main objects has been to determine when supersonic cracks traveling faster than the shear wave speed can occur. In contrast to subsonic cracks, the speed of supersonic cracks is best expressed as a function of strain, not stress intensity factor. Nevertheless, we find that supersonic cracks are more common than has previously been realized. They occur both in Mode I and Mode III, with or without anharmonic changes of interparticle forces prior to breaking, and with or without dissipation. The extent and shape of the supersonic branch of solutions depends strongly on details such as lattice geometry, force law anharmonicity, and amount of dissipation. Particle forces that stiffen prior to breaking lead to larger supersonic branches. Increasing dissipation also tends to promote the existence of supersonic states. We include a number of other results, including analytical expressions for crack speeds in the high-strain limit, and numerical results for the spatial extent of regions where particles interact anharmonically. Finally, we note a curious phenomenon, where for forces that weaken with increasing strain, cracks can slow down when one pulls on them harder.

Keywords Brittle fracture · Cracks · Lattice models · Exact solutions · Supersonic · Molecular dynamics · Wiener-Hopf

T. M. Guozden · E. A. Jagla
Centro Atómico Bariloche, Comisión Nacional de Energía Atómica, 8400 Bariloche, Argentina

M. Marder (✉)
Center for Nonlinear Dynamics and Department of Physics, The University of Texas at Austin, Austin, TX 78712, USA
e-mail: marder@chaos.ph.utexas.edu

1 Introduction

The terminal speed of cracks loaded in tension (Mode I) has been an object of curiosity for over 60 years. Calculations of Mott (1947) indicated that cracks should reach a maximum speed at a fraction of the shear wave speed, a conclusion that received support from experimental work of Schardin (1955, 1959). Theoretical study of energy flux to crack tips provided arguments that the maximum speed of a crack should be the Rayleigh wave speed c_R (Freund 1990; Broberg 1999), which is typically about 90% of the shear wave speed. Experimentally cracks do not usually reach this speed, and have terminal velocities that are around $0.6\,c_R$. This limit was eventually understood to result from instabilities of the crack tip that cause it to begin branching on small scales once the energy flux exceeds a critical value (Fineberg and Marder 1999). This line of argument leaves open however the question of what might happen if the crack-tip instabilities could be suppressed.

Both for Mode II and Mode III cracks, motion faster than the shear wave speed is known to be possible. In

Published online: 03 December 2009

the case of Mode II, Andrews (1976) first showed that intersonic motion (motion at speeds between shear and longitudinal wave speeds) was possible. A more comprehensive discussion including the effects of a tip cohesive zone was provided by Burridge et al. (1979) and the results are now well established in fracture mechanics (Broberg 1999). Rosakis et al. (1999) and Rosakis (2002) provided direct experimental confirmation. In the case of Mode III cracks, experimental evidence of supersonic rupture was provided by Petersan et al. (2004). Numerical and theoretical explanations involve the consideration of dissipative effects or spring nonlinearities, and were provided respectively by Marder (2005), Marder (2006) and Guozden and Jagla (2005). The experimental setting of the studies here described as Mode III is arguable; it is thin sheets of rubber, which when greatly stretched should obey the equations of Mode III elastodynamics. Rubber appears to suppress crack-tip instabilities spontaneously, perhaps because toughness is a strong function of the local stress state. This phenomenon is not yet well understood. However, the numerical and theoretical findings associated with the rubber rupture are unambiguous and led to two main conclusions.

1. Supersonic cracks in Mode III are possible so long as near-tip instabilities are suppressed.
2. The scaling behavior of supersonic cracks is different from that of subsonic cracks. For subsonic cracks, crack speed is a function of K/K_c (the ratio of stress intensity factor and fracture toughness) or equivalently of energy flux to the crack tip. For supersonic cracks, crack speed is a function of the strain in the vicinity of the crack tip, and conventional calculations involving energy flux are uninformative.

There has been evidence for some time that Mode I cracks can move at speeds above the Rayleigh wave speed as well. Following a study of the continuum mechanics of intersonic cracks, Slepyan and Fishkov (1981) obtained explicit analytical solutions for intersonic Mode I cracks in a lattice model (Kulakhmetova et al. 1984; Slepyan 2002). Buehler et al. (2003) also found intersonic cracks in molecular dynamics simulations, and they attributed the phenomenon to nonlinearities of the interatomic potentials.

Our goal in this paper is to extend these studies. We show that both supersonic and intersonic cracks occur quite generically in Mode I. We describe branches of intersonic and supersonic cracks in a variety of models. The Mode I cracks are like those in Modes II and III. Once near-tip instabilities are suppressed, supersonic crack motion occurs quite naturally. Like their Mode III counterparts, supersonic and intersonic cracks in Mode I are controlled by near-tip strain rather than by stress intensity factors. Many, although not all of the solutions Slepyan found are physically realizable. Abraham and Gao (2000) are correct in noting that details of the shape of interatomic potentials greatly affect crack speeds, but crack motion above the Rayleigh wave speed does not necessarily require hyperelasticity, and may occur even for strain softening potentials in the presence of dissipation.

The work in this paper is theoretical. We use two complementary numerical methods

1. The primary method is direct integration of Newton's equations of motion (molecular dynamics) for atomic systems whose atoms interact with forces that drop to zero past a critical extension and hence permit solutions that correspond to cracks. Here we restrict our study to force laws that are piecewise linear, and to cracks moving along the weakened center line of a strip. The numerical code can be run by letting bonds ahead of the crack break when a maximum extension is reached, or, in a slight variation, can allow bonds on the crack line to snap at specified time intervals. This last feature enhances the ability to compare with the Wiener-Hopf calculations described below.
2. The second is a method based on the Wiener-Hopf technique (Marder and Gross 1995; Noble 1958) that makes it possible to find the properties of cracks in steady states by performing some integrals. The advantage of this method is that it is very fast and is suited to finding the relationship between calculations at the atomic scale and the macroscopic limit. However, it is based on the assumption that bonds along a crack line break in sequence at a steady rate and can be employed only for a very specific class of interatomic forces, those that are linear up to the point of rupture.

By combining results from these two methods, we are able to obtain a fairly comprehensive picture of the existence of intersonic and supersonic cracks. As a synthesis of the results, and to serve as a guide for the rest of the paper, in Tables 1 and 2 we summarize the conditions under which supersonic propagation is obtained.

Table 1 Summary of qualitative conditions for subsonic or supersonic propagation

Regime	Mode	Conditions	Comments
Subsonic	III	δ/δ_G of order 1	See Fig. 2
	I	Any δ	δ Has to be increased slowly to stay on this branch. See Sect. 4
Supersonic	III	δ/δ_C finite	See Fig. 2. For analytical expressions for the divergence as $\delta \to \delta_C$ see (Fig. 6)
	I	$\delta/\delta_C \gtrsim 0.75$	Finding these states requires proper choice of initial conditions, which include changing δ suddenly, giving large velocity to near-tip masses, or starting at large strains and slowly decreasing δ. See Fig. 7. Some supersonic regimes can be achieved by changing the breaking sequence in square lattices, as shown in Figs. 11 and 12
	I and III	$\gamma > 1$, δ/δ_C finite	See Fig. 19
	I and III	Finite dissipation (Kelvin or Stokes), δ/δ_C finite	Singularities near the crack tip similar to stiffening nonlinearities, which may drive the crack supersonically. See Sect. 4.1

The scaled values δ/δ_C and δ/δ_G are defined in Eqs. (17) and (16). γ is defined in Eq. (23). System is always harmonic ($\gamma = 1$) and no dissipation is present except when explicitly stated

Table 2 Summary of quantitative conditions leading to supersonic cracks in lattices

Lattice	Mode	Non-linearity	Minimum scaled strain δ/δ_C	Comments
Triangular	III	None	0.24	Wiener–Hopf computation in systems 4,000 rows high
Square	III	None	0.95	Wiener–Hopf computation in systems 4,000 rows high
Triangular	I	None	0.76	Molecular dynamics computations in systems 20–80 high
Square	I	None	0.62	Molecular dynamics computations in systems 80 high
Triangular	I	Stiffening ($\gamma = 2.$)	0	Molecular dynamics computations in systems 20–180 high. The minimum strain continuously decreases as system size increases
Triangular	I	Softening ($\gamma = 0.5$)	0.62	Molecular dynamics computations in systems 20–40 high

In all cases, the threshhold for appearance of supersonic states must be expressed in terms of a minimum scaled strain δ/δ_C rather than fracture energy, or stress intensity factor. The scaled strain δ/δ_C is defined in Eq. (17). γ is defined in Eq. (23). Results are given in absence of dissipation; dissipation changes quantitative values

The structure of the paper is as follows:

Section 2: We review the properties of ideal brittle solids that form the setting for our work.

Section 3: We review the scaling structure of subsonic and supersonic cracks in Mode III and provide some new results, including an analytical expression for the speeds of supersonic cracks in triangular and square lattices.

Section 4: We examine the scaling structure of Mode I solutions and demonstrate the existence of a branch of supersonic solutions.

Section 5: We extend the numerical studies to consider hyperelastic potentials between atoms and determine their effect upon the various branches of crack motion.

Section 6: Conclusions.

2 Details of the model

We focus on two-dimensional systems formed by single layers of particles in a strip. The strip lies in the x–y plane, with the axis along the x direction as shown in Fig. 1. The dynamic variables of the problem are

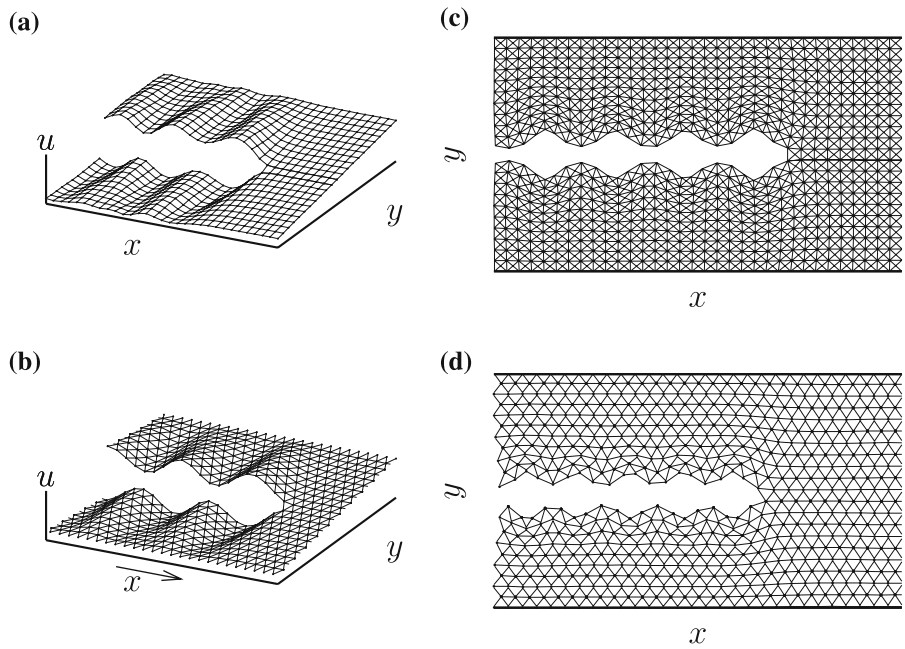

Fig. 1 Sketch of cracks propagating in mode III in: **a** a square lattice, **b** a triangular lattice; and in mode I in: **c** a square lattice, **d** a triangular lattice

the displacements of lattice points with respect to their equilibrium positions. There is a single out-of-plane displacement u_i for mode III conditions (i labels both x and y coordinates at equilibrium), and there are two in-plane displacements $\boldsymbol{u}_i \equiv (u_i^x, u_i^y)$ for mode I. We consider both square and triangular lattices. The net force f_i on a given node i is calculated at each time by summing up the contributions of all springs connecting to that node. The explicit expressions for mode III and mode I follow.

2.1 Mode III

For mode III we have for the force f_i on particle i

$$f_i = \sum_j \phi(u_{ij}). \tag{1}$$

where

$$u_{ij} = u_j - u_i.$$

We begin by taking the forces between neighbors to have an ideal brittle form that remains linear up to the breaking point. Both for triangular and square lattices, we take

$$\phi(u_{ij}) = \begin{cases} ku_{ij} & \text{if } i \,\&\, j \text{ are nearest nbrs not on center line} \\ 0 & \text{if } i \,\&\, j \text{ are not nearest neighbors} \\ ku_{ij}\,\tilde{\theta}(u_{\mathrm{bk}} - |u_{ij}(t)|) & \text{if} i \,\&\, j \text{ are nearest nbrs across center line} \end{cases} \tag{2}$$

Here k is the lattice spring constant, and u_{bk} is an extension past which points spanning the crack line break due to the Heaviside function $\tilde{\theta}$. The reason for the decoration on $\tilde{\theta}$ is that we take the Heaviside function to depend upon the complete history of the bond extension $u_{ij}(t)$. Once a bond stretches to a distance greater than u_{bk} the force between the two particles drops irreversibly to zero and never appears again even if the particles come back into contact. This choice mimics irreversibility due to conformational changes in brittle glasses and polymers. Thus there is a weakened plane running across the center of the strip where bonds can break and permit a crack to run. Weak planes can be realized experimentally, for example by gluing two pieces of material together, or by fracturing crystals. We have deliberately chosen only to allow fracture along the weak plane so as to suppress instabilities that would otherwise arise (Fineberg and Marder 1999).

2.2 Mode I

For mode I, we work in the limit of infinitesimal displacements, namely where displacements are small compared to the equilibrium lattice spacing. Thus the two component force $\boldsymbol{f} = (f^x, f^y)$ is given in this case by

$$\boldsymbol{f}_i = \sum_j \phi(u_{ij})\ \boldsymbol{n}_{ij}, \tag{3}$$

where

$$\boldsymbol{n}_{ij} = (\boldsymbol{u}_j^0 - \boldsymbol{u}_i^0)/|(\boldsymbol{u}_j^0 - \boldsymbol{u}_i^0)|$$

is the constant unit vector joining the original equilibrium positions of nodes j and i and

$$u_{ij} = |\boldsymbol{u}_{ij}|; \quad \boldsymbol{u}_{ij} = \boldsymbol{u}_j - \boldsymbol{u}_i.$$

For triangular lattices in Mode I, we take

$$\phi(u_{ij}) = \begin{cases} ku_{ij} & \text{if } i \,\&\, j \text{ are nearest nbrs not on center line} \\ 0 & \text{if } i \,\&\, j \text{ are not nearest neighbors} \\ ku_{ij}\tilde{\theta}(u_{\rm bk} - |u_{ij}(t)|) & \text{if } i \,\&\, j \text{ are nearest nbrs across center line} \end{cases} \tag{4}$$

while for square lattices in Mode I we take interactions up to second neighbors in the form

$$\phi(u_{ij}) = \begin{cases} ku_{ij} & \text{if } i \,\&\, j \text{ are near nbrs not on crack line} \\ ku_{ij}/2 & \text{if } i \,\&\, j \text{ are 2nd nbrs not on crack line} \\ 0 & \text{if } i \,\&\, j \text{ are further than 2nd nbrs} \\ k\,u_{ij}\tilde{\theta}(u_{\rm bk} - |u_{ij}(t)|) & \text{if } i \,\&\, j \text{ are near nbrs across crack line} \\ ku_{ij}/2\tilde{\theta}(u_{\rm bk}/\sqrt{2} - |u_{ij}(t)|) & \text{if } i \,\&\, j \text{ are near nbrs across crack line} \end{cases} \tag{5}$$

The reason for choosing this particular second neighbor interaction is to obtain an elastically isotropic square lattice in linear elasticity.

2.3 Dynamics and other details

The force on each node is evaluated at each time step, and it is used to integrate the corresponding Newton equation of motion, namely

$$m\frac{\partial^2 u_i}{\partial t^2} = f_i \quad \text{mode III} \tag{6}$$

$$m\frac{\partial^2 \boldsymbol{u}_i}{\partial t^2} = \boldsymbol{f}_i \quad \text{mode I} \tag{7}$$

where m is the mass associated with each node.

The system is composed of L_y rows along the y direction, and L_x sites on each row. The driving force for crack propagation is imposed as a constant displacements on top and bottom rows, namely those for which

$$u_i^y = 0 \text{ (bottom)} \tag{8}$$

$$u_{i'}^y = (L_y - 1)a\ (\sqrt{3}/2) \text{ (top, triangular lattice)}$$

$$u_{i'}^y = (L_y - 1)a \text{ (top, square lattice)},$$

where a is the lattice constant.

Here i and i' label points so that u_i and $u_{i'}$ are at the same horizontal position but on the bottom and top rows respectively and a is the lattice parameter. To describe the driving force for crack motion, we define δ to be the nominal displacement from equilibrium between vertical rows ahead of the crack. The imposed displacements are

$$u_{i'} - u_i = \delta \tag{9}$$

for mode III, and

$$u_{i'}^y - u_i^y = \delta \tag{10}$$

$$u_{i'}^x - u_i^x = 0 \tag{11}$$

for mode I.

In mode I, on the left and right borders of the system we impose a variety of boundary condition; sometimes $u_{0,j}^x = u_{L_x,j}^x = 0$ and at other times a damping region (Marder 2004). We use values of L_x ranging from $2L_y$ to $4L_y$.

As springs break during the simulation we shift the system to the left, so the crack tip remains near the center of the simulation lattice. This is done by adding a new columns at the right of the system (ahead of the crack), and deleting left columns (behind the crack). Crack velocity is measured as the average rate of spring breaking.

To this point we have not referred to dissipative terms in our simulations. In the absence of strong dissipative effects the kinetic energy released by the crack

travels to the left hand side of the system and either decays in a damping region or is removed when columns of material are discarded. We have verified that our results do not depend upon the details of how the left and right boundaries are treated. Note that in most treatments of Linear Elastic Fracture Mechanics, energy dissipation mechanisms are supposed to be present so that high-frequency kinetic energy generated by the crack advance is dissipated in an infinitesimal neighborhood of the crack tip. This means that the generation of kinetic energy in our model can be considered to be part of the crack energy as usually defined in textbooks. Moreover, the increase of crack energy with crack velocity is accounted for in our model precisely by the generation of kinetic energy in high-frequency modes.

Nonzero dissipation is known to produce or enhance supersonic propagation (Marder 2005). We have conducted some studies with phenomenological Kelvin and Stokes dissipation. The equations of motion for the Kelvin case are

$$m\frac{\partial^2 u_i}{\partial t^2} = \left(1+\beta\frac{\partial}{\partial t}\right) f_i \quad \text{mode III} \tag{12}$$

$$m\frac{\partial^2 \boldsymbol{u}_i}{\partial t^2} = \left(1+\beta\frac{\partial}{\partial t}\right) \boldsymbol{f}_i, \quad \text{mode I} \tag{13}$$

and for the Stokes dissipation case

$$m\frac{\partial^2 u_i}{\partial t^2} = f_i - \beta\frac{\partial u_i}{\partial t} \quad \text{mode III} \tag{14}$$

$$m\frac{\partial^2 \boldsymbol{u}_i}{\partial t^2} = \boldsymbol{f}_i - \beta\frac{\partial \boldsymbol{u}_i}{\partial t}. \quad \text{mode I} \tag{15}$$

Unless otherwise stated, the results presented correspond to the limit of vanishingly small β.

These equations are not quite accurately expressed; we do not allow the time derivative $\beta\partial/\partial t$ to act on the θ function when bonds snap. As bonds snap we send the force due to the snapping bond immediately to zero, both in numerical routines and in the Wiener–Hopf solutions. This choice avoids unphysical singularities in the force at the moment of bond rupture.

Under mode III conditions, there is a single characteristic velocity c for the propagation of elastic disturbances For our square and triangular lattices the wave speeds are $c = a\sqrt{k/m}$ and $c = a\sqrt{3k/2m}$ respectively, where a is the lattice parameter. These wave speeds are computed by finding the long-wavelength limit of the phonon spectrum for the lattice.

In mode I there are two primary wave speeds: shear (c_S) and longitudinal (c_P). In terms of the elastic constants of the bulk material, the shear wave velocity is related only to the shear modulus since it involves only constant volume perturbations, whereas the longitudinal wave velocity depends both on the shear and bulk modulus of the material. It always turns out that $c_S \leq c_P$. In our lattices, the values obtained for the wave speeds are $c_S = a\sqrt{3k/8m}, c_P = 3a\sqrt{k/8m}$ for the triangular lattice, and $c_S = a\sqrt{k/2m}, c_P = a\sqrt{3k/2m}$ for the square lattice. Note that both lattices have the same relation $c_S/c_P = 1/\sqrt{3}$ and thus the same Poisson coefficient $\nu = 1/3$.

An additional very important velocity in mode I crack propagation problems is that known as the Rayleigh velocity c_R (Broberg 1999). This is the velocity at which elastic waves propagate along a free boundary of the system (which can be the crack surface). This velocity is a well defined function of the ratio c_S/c_P. For our lattices we obtain $c_R = \sqrt{\frac{2}{3}\left(3-\sqrt{3}\right)}c_S \simeq 0.9194\, c_S$.

In a constant displacement experiment in a strip geometry, there are two important values of the displacement δ that play a special role in all the analysis. One is the Griffith displacement δ_G

$$\delta_G = \begin{cases} \frac{2}{\sqrt{3}}u_{\mathrm{bk}}/\sqrt{L_y-1} & \text{triangular lattice,} \\ & \text{Modes I and III} \\ u_{\mathrm{bk}}/\sqrt{L_y-1} & \text{square lattice,} \\ & \text{Modes I and III} \end{cases} \tag{16}$$

where the elastic energy stored in a unit length of material in the direction of crack advance equals the energy of a spring at the rupture point. Crack propagation cannot occur for $\delta < \delta_G$. The second important displacement value is that at which even a strip with no seed crack breaks. This value δ_C is called the limit of uniform breakdown, and is independent of the strip height L_y:

$$\delta_C = \begin{cases} \frac{2}{\sqrt{3}}u_{\mathrm{bk}} & \text{triangular lattice, Modes I and III} \\ u_{\mathrm{bk}} & \text{square lattice, Modes I and III} \end{cases} \tag{17}$$

3 Mode III (tearing mode)

In this section we study the dependence of crack velocity on displacement δ for a crack propagating in systems of different widths under mode III conditions, extending the studies of previous authors (Marder 2005, 2006; Kessler 1999, 2000).

Literal realizations of Mode III fracture, where masses travel only perpendicular to their original

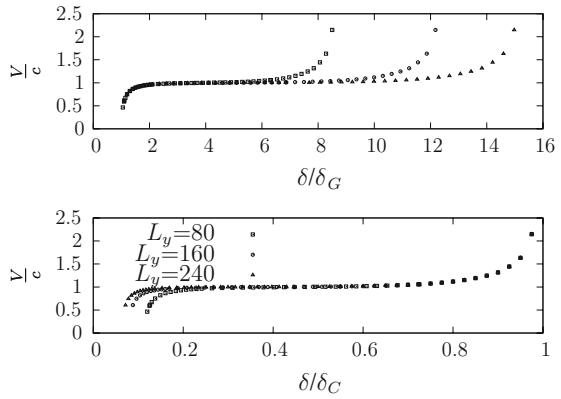

Fig. 2 Velocity of a mode III crack running on triangular lattices with different number of rows. Note that the plot as a function of δ/δ_G produces the collapse of the data for $V < c$, whereas for $V > c$ the collapse is produced by preparing the plot as a function of δ/δ_C. δ_G and δ_C are defined in Eqs. (16) and (17)

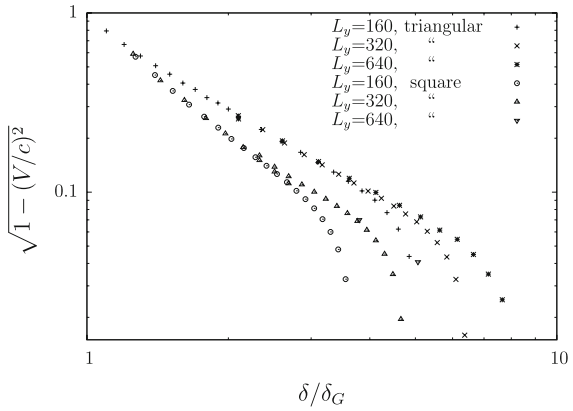

Fig. 3 The same data as in Fig. 2, plus the equivalent ones obtained in a square lattice, plotted in a way that suggests a power law dependence for $V \to c$

locations in a very thin sample, are experimentally difficult to achieve. Theoretically, this configuration allows one to explore all the concepts that appear in the more physical Mode I case with much less formal complexity. In addition, the in-plane rupture of rubber can be described by Mode III equations to a surprisingly high degree of accuracy.

In Fig. 2 we plot the results of our simulations for triangular lattices. Two well defined regimes can be observed: when the crack velocity is lower than the wave speed in the system c, the dependence of the results on the width of the system can be absorbed by plotting V as a function of δ/δ_G (Fig. 2a). However, there is a regime in which $V > c$, and to scale the results in this case the plot has to be prepared in terms of δ/δ_C (Fig. 2b). We analyze now both regimes separately.

The plot in terms of δ/δ_G shows that for 'macroscopic' samples ($L_y \to \infty$) V is a function of δ/δ_G that asymptotically reaches the wave speed c. It is useful to combine this result with those provided by LEFM. In this framework, assuming a stationary propagation of a crack with some velocity V, a well defined relation is obtained between the energy flux to the crack tip $\mathcal{E}$ per unit of crack advance, and the amplitude of the most singular term of the stress field close to the crack tip. This amplitude (appropriately normalized) is the stress intensity factor $K_{\rm III}$. The result obtained in LEFM for Mode III configurations is (Broberg 1999; Field and Baker 1961)

$$\mathcal{E} = \frac{K_{\rm III}^2}{2\mu\sqrt{1-(V/c)^2}}. \tag{18}$$

In the strip configuration with fixed displacement boundary conditions the energy flux $\mathcal{E}$ is simply given by the elastic energy stored in a unit length well ahead of the crack. Thus

$$\mathcal{E} = \mathcal{E}_0(\delta/\delta_G)^2 \tag{19}$$

where $\mathcal{E}_0$ is the value of $\mathcal{E}$ at the Griffith threshold, In our case, $\mathcal{E}_0 = \frac{k}{a}u_{\rm bk}^2$ for the triangular lattices, and $\mathcal{E}_0 = \frac{k}{a}\frac{u_{\rm bk}^2}{2}$ for the square lattice. Combining Eqs. (18) and (19) we obtain

$$K_{\rm III} = \sqrt{2\mu\mathcal{E}_0}(1-(V/c)^2)^{1/4}\frac{\delta}{\delta_G} \tag{20}$$

The prediction of LEFM is limited to this expression. In particular it does not give the dependence of V on δ/δ_G, which is to be expected since it is dependent upon microscopic details. In Fig. 3 we see results for the triangular lattice of Fig. 2, along with the equivalent ones for a square lattice plotted in a slightly different form that allows one to infer a systematic power law dependence of $\sqrt{1-(V/c)^2}$ on δ/δ_G for large systems. Inserting these results into expression (20) we obtain the values of $K_{\rm III}$ as a function of V shown in Fig. 4.

We see how the simple change of lattice geometry produces important effects. Whereas $K_{\rm III}$ decreases with V and tends to a constant value for $V \to c$ for the

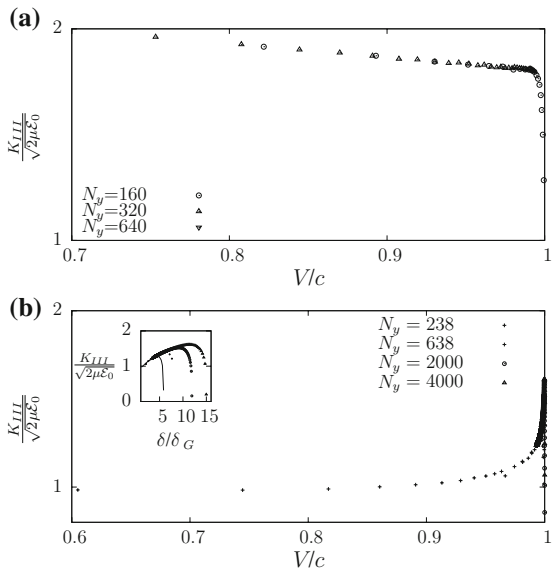

Fig. 4 Stress intensity factor K_{III} obtained from simulations of a crack propagating in a **a** square lattice; and **b** a triangular lattice. In *inset* in **b** we plot K_{III} versus δ/δ_G. Whereas K_{III} decreases with V and tends to a constant value for $V \to c$ for the square lattice, in a triangular lattice K_{III} increases with V and appears to have a weak divergence in the limit of infinite system size

square lattice, in a triangular lattice K_{III} increases with V and appears to have a weak divergence in the limit of infinite system size.

We now move to the analysis of the regime of δ close to δ_C. In this case we observe that the crack velocity can be larger than the wave velocity, and in particular it diverges as $\delta \to \delta_C$.

An analytical calculation allows us to obtain the form of the divergence of V for $\delta \to \delta_C$. As δ is very close to δ_C, all springs are very close to the rupture point, and a leading order calculation that considers the effect of the spring that is breaking on the next spring to be broken is enough to predict the velocity in this limit (see Fig. 5). Let us consider first the case of a triangular lattice. If a spring breaks at some time t_0, it produces a change $\Delta f = k\delta$ in the force on the points to which the spring was connected. This force increases progressively the length of the next spring to be broken as $\delta + \frac{\Delta f}{2m}(t-t_0)^2 = \delta\left(1 + \frac{k}{2m}(t-t_0)^2\right)$. When the length of this spring reaches the value δ_C it breaks, and this occurs at time $t_1 = t_0 + \frac{2}{\sqrt{k/m}}\sqrt{\delta_C/\delta - 1}$. Thus we obtain the velocity as $V = \frac{a/2}{(t_1-t_0)} = \frac{a\sqrt{k/m}}{2\sqrt{2}}\frac{1}{\sqrt{\delta_C/\delta - 1}}$. The calculation for the square lattice proceeds along the same lines; the main difference is that now the breaking of a spring does not produce an immediate effect on the next spring to be broken. Instead, the effect is mediated by the deformation of the connecting spring lying in the crack direction. This produces the result that the net force acting on the spring to be broken is not constant, but is proportional to $(t-t_0)^2$. A detailed calculation yields $V = a\sqrt{k/m}[12\,(\delta_C/\delta - 1)]^{-1/4})$. Numerical results of the divergence are compared with these analytic predictions in Fig. 6. Note that there are no free parameters in this fit. We see that the agreement is very good.

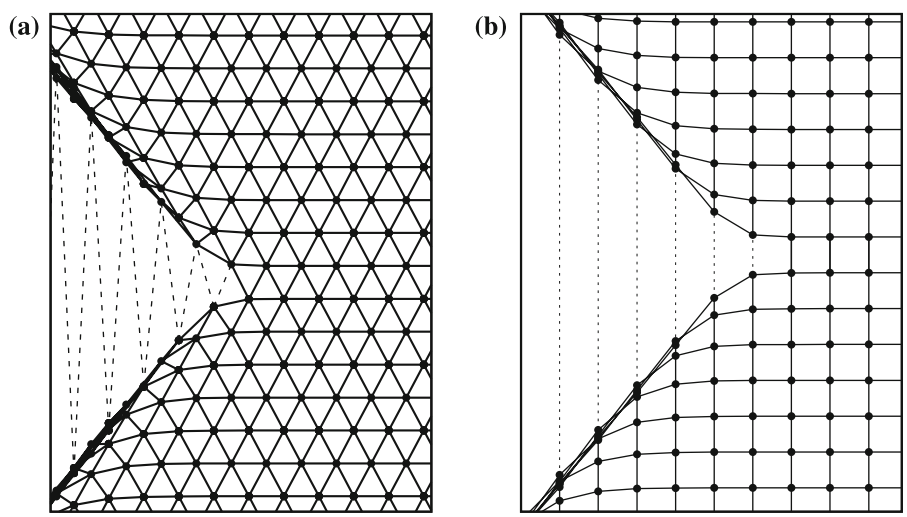

Fig. 5 Side view of a mode III crack propagating in the supersonic regime through a triangular lattice (**a**) and a square lattice (**b**)

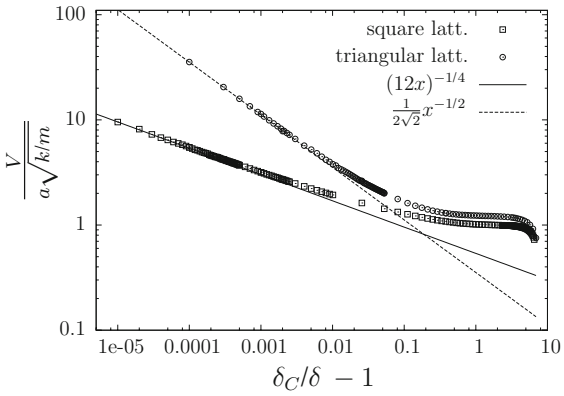

Fig. 6 Divergence of the velocity as the strain approaches the limit of uniform breakdown δ_C for square and triangular lattices (mode III). The system size is $L_y = 80$

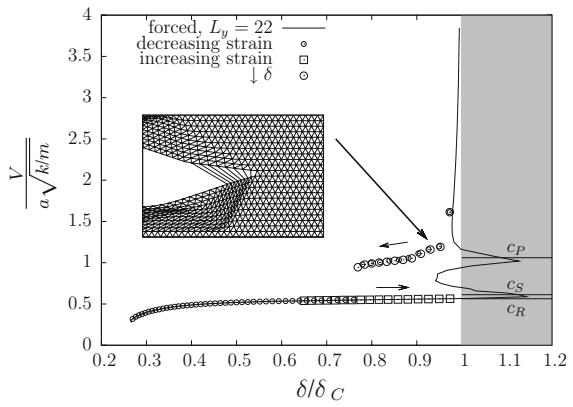

Fig. 7 Plot of the velocity V of a crack versus δ/δ_C, propagating on a triangular lattice with 21 rows of springs. The *arrows* show different behaviors: if we increase the strain slowly enough (*squares*), the velocity is bounded by c_R, but if the strain is suddenly changed to $\delta/\delta_C >\sim 0.95$ the system explores the supersonic regime. Decelerating from this state (*circles*), the system goes through an intersonic regime in which a symmetry-breaking rupture occurs as shown in the *inset*. We also show results (*line*) obtained by forcing the crack to propagate at a predefined velocity, cutting springs at the appropriate rate. The *shaded region* is physically not accessible as here energy is flowing from the crack tip to the system. The relevant sound velocities in the system are indicated.

4 Mode I (opening mode)

We now present results for lattices under mode I conditions. Some additional details about the implementation are needed in this case. We work again with both triangular and square lattices, in the infinitesimal approximation. In particular, displacements perpendicular to the spring direction do not produce forces on the particles. Remember that in this case, for square lattices we also have springs connecting second nearest neighbors, as shown explicitly in Eq. (5). In this case the crack breaks two different type of springs as it advances. Different models can be defined by proposing different breaking prescriptions of the two springs, as we will see later.

We first present results for the triangular lattice in Fig. 7, where we plot the velocity of the crack versus δ/δ_C. In this figure, different behaviors of the crack can be seen:

- if we increase the strain slowly enough, velocity remains bounded by c_R, even if $\delta \to \delta_C$.
- if we suddenly change the strain from a small value to $\delta/\delta_C \gtrsim 0.95$, we observe that propagation becomes supersonic.

With the system in the supersonic regime, and diminishing the strain, another change occurs: a rupture of symmetry along the line described by the crack propagation. We can see this asymmetry in the inset of Fig. 7. This asymmetry makes springs in front of the former crack tip also exceed the breaking threshold. We emphasize that the symmetry-breaking takes place at a microscopic level, but so far as continuum mechanics is concerned, one is observing an intersonic Mode I crack. Similar results are also plotted versus δ/δ_G and for different system sizes in Fig. 8.

In Fig. 7 we also show results (continuous line) obtained by forcing the crack to propagate at a predefined velocity, cutting springs at the appropriate rate. We measure the springs length at the moment we cut them, and rescale the value to obtain δ/δ_C. We see that the length of the spring goes to zero (δ/δ_C very large) when the velocity is set to c_R, c_S or c_P. The region where $\delta/\delta_C > 1$ is shaded because it is not physically accessible, as energy flows from the tip to the system. This results are very similar to the ones obtained by the Wiener Hopf method (Marder and Gross 1995; Noble 1958), which supposes a crack running at a constant speed. We see a comparison between the methods in Fig. 9. The slight discrepancy above c_R corresponds to small differences between the length of consecutive springs at the moment of cutting in the numerical system. This difference is not allowed in the exact solution obtained by the Wiener Hopf method, and this explains the discrepancy.

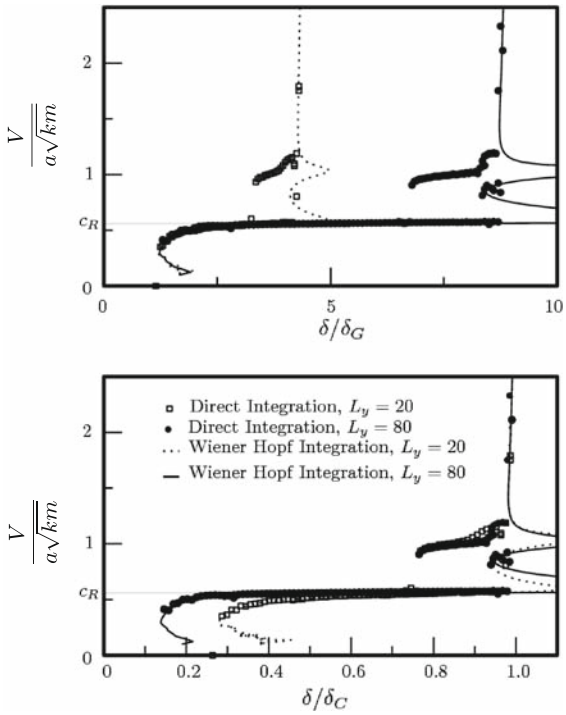

Fig. 8 Velocity of a crack propagating in triangular lattices, plotted against δ/δ_C and δ/δ_G for different system sizes. The *top panel* shows crack velocity as a function of δ/δ_G, which produces scaling results for subsonic cracks. The *lower panel* shows crack velocity as a function of δ/δ_C, which produces scaling results for supersonic cracks. We show results from direct integration for systems of size 20 and 80 compared with results of Wiener–Hopf integration Dissipation is negligible, and the breaking distance $u_{\rm bk}$ for the direct integration is 1.015

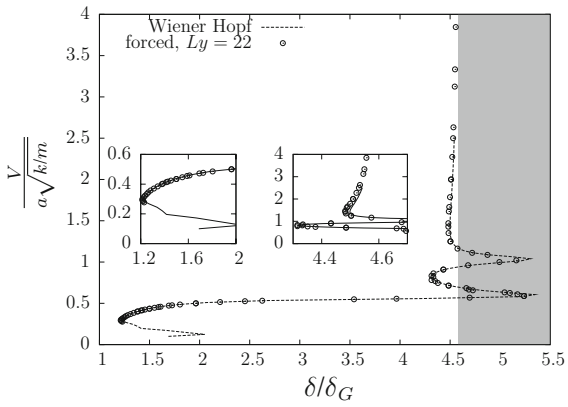

Fig. 9 Comparison between the forced propagating method and the Wiener Hopf method. The results agree except for a slight discrepancy above c_R. In the forced method we find small differences between the length of consecutive cut springs, although this does not occur in the exact solution found by the Wiener Hopf method. The difference is insignificant. We show in the *insets* the regions near $\delta/\delta_G \to 1$ and $\delta/\delta_C \to 1$

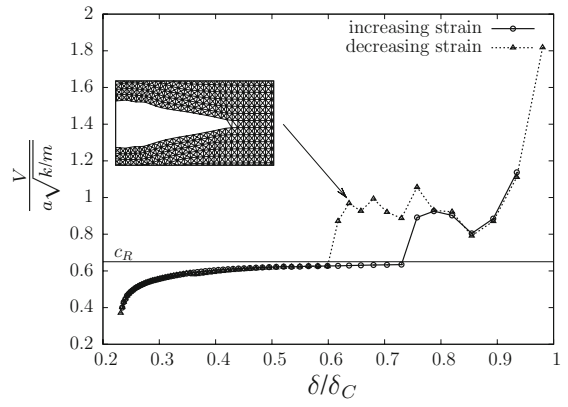

Fig. 10 Crack propagating in a square lattice. The behavior is similar to that in Fig. 7. The difference is that when slowly increasing the strain, the velocity is not bounded by c_R: asymmetric rupture occurs along the *line* defined by the crack, for the intersonic states as shown in the *inset*. Again, some springs in front of the crack tip may overpass the breaking threshold

In Fig. 10 we present results of a crack propagating in a square lattice. As in the previous simulations only springs in the middle row break. The main difference here is that we have springs linking second neighbors, which we will call diagonal springs. Vertical springs (linking first neighbors) are cut if they are stretched above $u_{\rm bk}$, and diagonal springs (linking second neighbors) break if their length is above $u_{\rm bk}/\sqrt{2}$. The behavior is similar to that found in Fig. 7, except that the velocity does not remain bounded by c_R while increasing the strain in the subsonic regime. A symmetric rupture occurs and propagation accelerates.

To see the dependence upon the breaking rule in square lattices, we study a different breaking sequence. Measuring the length of only the vertical spring at the crack tip, when this spring stretches above $u_{\rm bk}$, we cut it together with the two next diagonal springs. We have seen that in this case asymmetric ruptures do not occur. This was checked by re-running the simulations in symmetrically forced systems and obtaining the same results. We can compare spontaneous cracks with points obtained by forced propagation (Fig. 10). The behavior is the same as in the triangular case: when increasing slowly the applied strain, the velocity remains bounded by c_R. To enter the supersonic regimes, an initial condition with $\delta/\delta_C > 0.9$ needs to be established (Fig. 11).

Yet another breaking rule could be considered. In this case we sum up the energy of vertical and

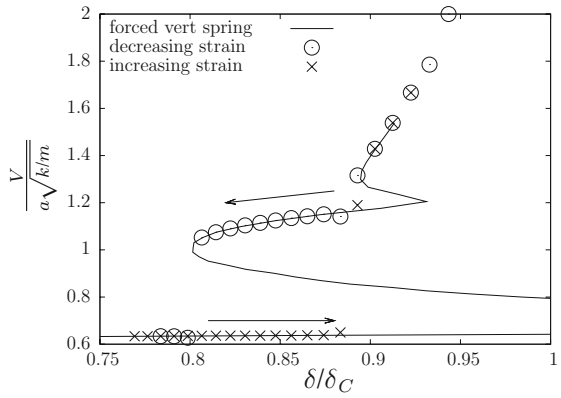

Fig. 11 Spontaneous and forced propagation in a square lattice, using a breaking rule involving only vertical springs. The system is always symmetrical in this case: we obtained the same solutions by rerunning the simulations in symmetrical systems with respect to the crack propagation line. When increasing slowly the applied strain, the velocity remains bounded by c_R. To enter the supersonic regimes, we made a sudden change in strain into $\delta/\delta_C > 0.9$. The crack remains in the supersonic regime while the applied strain decreases, switching first to the intersonic branch at $\delta/\delta_C \sim 0.9$, and finally to a subsonic branch at $\delta/\delta_C \sim 0.8$

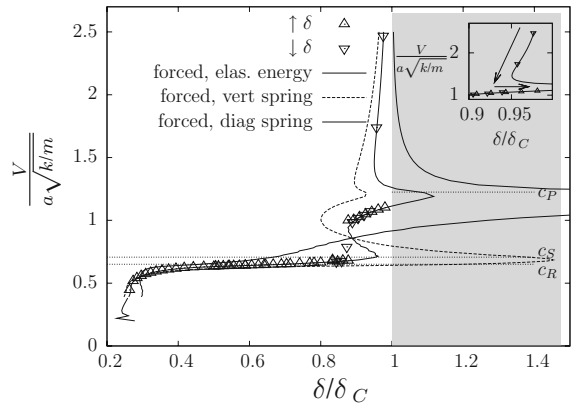

Fig. 12 Results in a square lattice, with a breaking rule that measures the energy of together vertical and diagonal springs. We show also the results of forced propagation, where we plot the energy of together the vertical and diagonal springs and their separate lengths

diagonals springs. When this total elastic energy goes above a prescribed threshold we cut the three springs together, as in the previous method. The main difference is that the strain in the direction of propagation is now part of the rule. This component is relevant, as we see that when the velocity approaches c_R there is an expansion in the crack propagation direction, together with a compression in the perpendicular direction. In Fig. 12 we show results obtained with this rule and also the ones obtained by forced propagation. Once again we see hysteretic behavior, with non-symmetric rupture. Note that the velocity is not bounded by c_R in this case.

4.1 Dissipation

To address the effect of dissipation, we have used Kelvin and Stokes dissipation terms, as described in Eqs. (12), (13), (14) and (15). It should be noticed that when studying the effect of the system size on crack propagation, the coefficient β must be rescaled carefully to get sensible results in the limit of large system sizes. For a given value of δ/δ_G, the Stokes dissipation parameter should be scaled as $\beta^{(S)} \sim 1/L_y$ (Fig. 13), whereas Kelvin dissipation parameter $\beta^{(K)}$ should remain constant (Fig. 14).

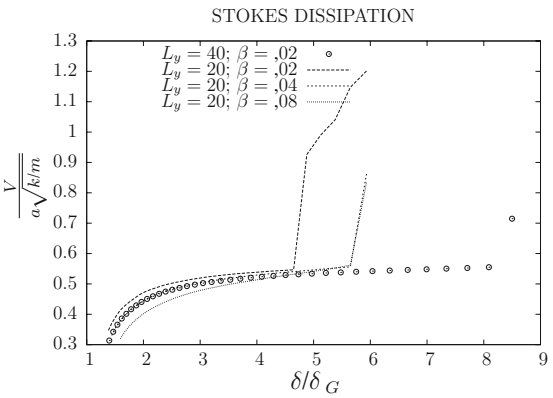

Fig. 13 Mode I velocity of crack propagation as a function of δ/δ_G in presence of Stokes dissipation. If we increase the size of the system we have to proportionally reduce the dissipation to obtain the same results for the same fracture energy δ/δ_G. See that for same size L_y the velocity is always reduced in the harmonic case, with the exception of softening nonlinearities as shown in Fig. 26

The effects of finite dissipation on crack velocity are not totally intuitive. Stokes dissipation always decreases the speed of the crack, with the exception of the softening nonlinearities case as seen in Fig. 25. Stokes dissipation never produces supersonic propagation. In contrast, Kelvin dissipation may increase the velocity over c_R in some cases. This raises the possibility that dissipation by itself can expand the range of supersonic crack solutions. As shown in Fig. 14, this does not happen in the macroscopic limit. For any fixed dissipation

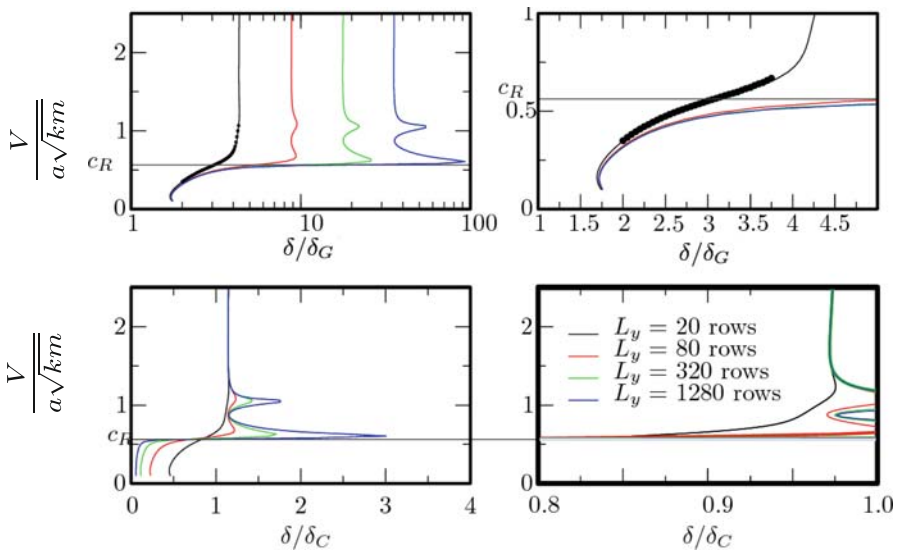

Fig. 14 Crack velocity versus loading for four different system heights L_y, and plotted both as a function of δ/δ_G and δ/δ_C to bring out subsonic and supersonic states respectively for dissipation $\beta = 1$. The curves are produced with the Wiener–Hopf method except for the system of height $L_y = 20$, where the filled circles represent direct numerical integration of the equations of motion for comparison. For different L_y and same β the results scale for the same fracture energy δ/δ_G

parameter β, as the system size increases, the lowest branch of crack solutions descends below the Rayleigh wave speed c_R. In classical fracture mechanics, Kelvin viscosity produces singular terms near the crack tip that are more divergent than the standard near-tip singularities, and therefore must be interpreted as part of the process zone. Essentially, Kelvin viscosity increases the fracture energy, and introduces a new length scale into the fracture problem that for $\beta = 1$ has grown comparable in size to the lattice spacing, and for larger β becomes larger. Thus increasing β has an effect similar to the effect of increasing $u_{\rm bk}$ and increasing the lattice spacing, but does not fundamentally change the nature of fracture solutions.

4.2 Energy and stress intensity factor

The plot of velocity as a function of δ/δ_G can be analyzed in the same manner we did for Mode III, for the subsonic branches in the triangular lattice and the square lattice (with the breaking rule for the vertical spring only). In particular, assuming a crack propagating in stationary conditions in a continuum system at a velocity $V < c_R$, an expression for the energy $\mathcal{E}$ flowing toward the crack tip is obtained from LEFM in the form (Broberg 1999; Nilsson 1972)

$$\mathcal{E} = \frac{K_I^2 Y_I(V)}{4(1-(c_S/c_P)^2)\mu} \tag{21}$$

where $Y_I(V)$ is called a Yoffe function. It has a divergence at $V = c_R$ and becomes negative for $c_R < V < c_S$. As in mode III, for all $V < c_R$, the energy transferred to the crack tip equals the elastic energy available in the system. Proceeding as in mode III (Eq. 19) we can thus write

$$K_I = \delta/\delta_G \sqrt{\frac{4(1-(c_S/c_P)^2)\mu\mathcal{E}_0}{Y_I(V)}} \tag{22}$$

Inserting in this expression the results from the simulations we obtain the dependence of K_I on δ/δ_G. The results are shown in Figs. 15 and 16 and point again to the existence of notable differences depending on the precise lattice geometry. While K_I is almost constant for the triangular lattice, it goes to zero as $V \to c_R$ for the square lattice. It must be mentioned however that this result changes if other breaking rules are used.

5 Additional elastic nonlinearities

In the preceding sections we have discussed the way in which a crack propagates when springs are perfectly linear up to the rupture point. We have found in particular that so long as crack branching is inhibited, the crack velocity increases as a function of the applied

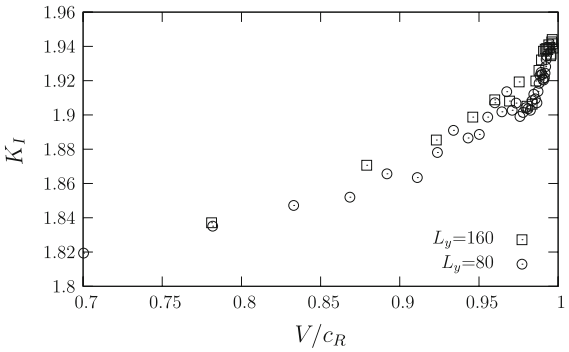

Fig. 15 Dependence of K_I (in units of $[\sqrt{\mu\mathcal{E}_0}]$) on V/c_R, for a triangular lattice. Note that K_I changes <10% in all the velocity range plotted

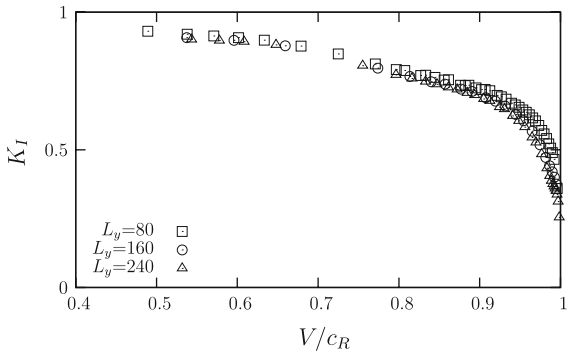

Fig. 16 Dependence of K_I (in units of $[\sqrt{\mu\mathcal{E}_0}]$) on V/c_R for a square lattice. In contrast with the result in the triangular lattice, we find that K_I seems to go to zero as $V \to c_R$

displacement δ and that both subsonic and supersonic branches of crack motion exist in all cases.

This picture is modified when the springs are not perfectly harmonic. Experiments (Rosakis et al. 1999; Sharon and Fineberg 1999; Petersan et al. 2004; Marder 2005) show that crack velocity can exceed the limit predicted by standard fracture mechanics. Broberg (1999), Freund (1990), Buehler et al. (2003), and Buehler and Gao (2006) showed when the spring constant becomes stiffer or softer at large extensions, the relationship between loading and crack velocity changes. The most spectacular results concerns the case of stiffening springs, in which case the extent of supersonic branches is greatly enlarged. We have made a detailed analysis of this problem in a mode III configuration in a previous publication (Guozden and Jagla 2005).

Here we make a systematic study of the velocity of cracks propagating in mode I configurations in the presence of non-linearities. The most remarkable results we obtain are the following. For stiffening of the springs at large stretching we find an extensive supersonic branch similar to one previously found for mode III configurations (Guozden and Jagla 2005). We also show that in the absence of dissipation, the size of the anharmonic zone scales as the width of the system, i.e., it occupies always a finite fraction of the system width. However, if some dissipation is included in the model, the size of the anharmonic region saturates for large width values, whereas the effect on the velocity is small. In this way, a situation can be obtained in which we have supersonic crack propagation driven by a spatial region which can be made arbitrarily small compared to the total system size. Finally, whether springs are softening or stiffening, there is always a supersonic crack branch as a function of δ/δ_C. In the macroscopic limit, this branch extends down to $\delta/\delta_C = 0$ for stiffening springs, but exists only for $\delta/\delta_C \gtrsim .5$ for softening springs.

For softening of springs at large stretching and in the subsonic regime, we find a systematic decrease of velocity, and in a narrow but robust region of parameters we find a propagation velocity that is a *decreasing* function of δ.

To account for spring non-linearities the definition in Eq. (4) is changed to (see Fig. 17).

$$\phi_{ij}(u_{ij}) = \begin{cases} ku_{ij} & \text{if } i \text{ and } j \text{ near neighbors and } u_{ij} < u_{\rm nl} \\ ku_{\rm nl} + \gamma k(u_{ij} - u_{\rm nl}) & \text{if } i \text{ and } j \text{ near neighbors and } u_{ij} > u_{\rm nl} \\ 0 & \text{if } i \text{ and } j \text{ not near neighbors} \\ ku_{\rm nl} + \gamma k(u_{ij} - u_{\rm nl}) & \text{if } i \text{ and } j \text{ near neighbors not across center line and } u_{\rm nl} < u_{ij} < u_{\rm bk} \\ 0 & \text{if } i \text{ and } j \text{ near neighbors across center line and } u_{ij} > u_{\rm bk} \end{cases} \tag{23}$$

The parameter $u_{\rm nl}$ is the length at which the spring constant γk kicks in. For stiffening systems, $\gamma > 1$ while for softening systems, $\gamma < 1$. In the runs we describe here, we have taken $u_{\rm nl}/u_{\rm bk} = 1/2$.

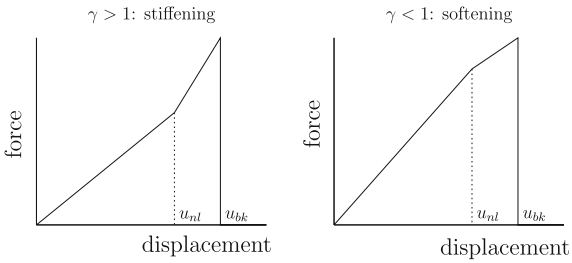

Fig. 17 Interaction between neighbors mass points as a function of displacement from equilibrium. At low deformations the behavior is harmonic, until the value $u_{\rm nl}$ is reached. Then it goes to a softer or stiffer regime depending on the parameter γ, until the spring breaks at $u_{\rm bk}$ (breaking is implemented only in the springs lying in the central row of the system)

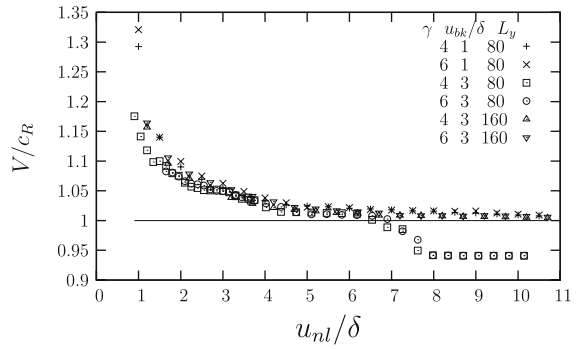

Fig. 19 Results for the velocity as a function of $u_{\rm nl}/\delta$ for different values of γ, $u_{\rm bk}/\delta$ and system width. L_y. The results for different parameters coincide within our numerical precision. Note that the values that drop below the $V = c_R$ line correspond to a small system with large $u_{\rm nl}$, and in that case there is no spring exploring the non-linear regime)

5.1 Hyperelastic stiffening

Figure 18 shows a characteristic plot of crack velocity v versus extension δ/δ_C for nonlinearity $\gamma = 4$, compared to the harmonic case, where nonlinearity sets in at $u_{\rm nl}/u_{\rm bk} = 1/2$. The presence of nonlinearity takes the branch that always lay below the Rayleigh wave speed for $\gamma = 1$ and moves it up so that it lies above. Thus hyperelastic stiffening promotes supersonic crack motion and makes supersonic motion possible for a wide range of conditions.

In a previous publication (Guozden and Jagla 2005) we studied in detail the velocity of cracks propagating in systems with hyperelastic stiffening under mode III conditions. On purely dimensional grounds the velocity of a crack in our model is in general a function of the ratios $\delta/u_{\rm nl}$, $\delta/u_{\rm bk}$, the system width w, and the anharmonicity parameter γ. We showed that when the crack propagates supersonically in mode III, it is natural to expect independence of velocity from the lateral size of the system, since no elastic disturbance can travel from the crack tip to the border and return to the crack tip. Thus the existence of the border cannot have any effect on the propagation velocity. From this type of analysis we concluded that once cracks go supersonic the velocity is independent of L_y. Moreover, additional considerations (see Guozden and Jagla 2005) suggested that the velocity is also largely independent of γ and $\delta/u_{\rm bk}$; i.e., it is determined by the value of $\delta/u_{\rm nl}$ alone.

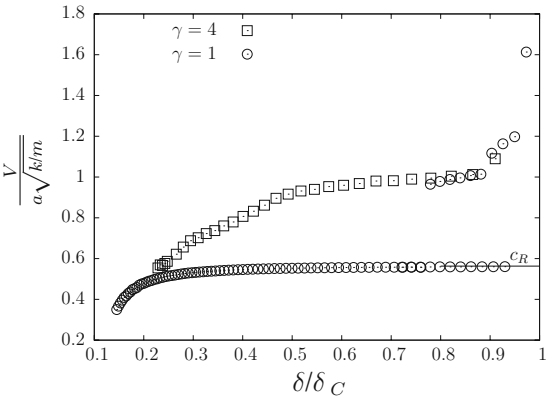

Fig. 18 Plot of crack velocity v versus extension δ/δ_C for nonlinearity $\gamma = 4$, compared to the harmonic case (including both branches) for a system of $L_y = 22$ rows. The presence of hyperelastic stiffening clearly enhances the velocity above c_R

We find the same behavior in the present simulations in Mode I: for large enough system sizes and large enough nonlinearity γ the crack velocity rises above c_R and results under many conditions can be collapsed when plotted against $u_{\rm nl}/\delta$ (Fig. 19), independent of the precise values of $u_{\rm bk}/\delta$, w, and γ. This is a bit surprising because in mode I compression waves exist in the system that propagate faster than the crack, and they can in principle travel to the border and return back to the crack tip, providing information to the crack tip about the width L_y of the system. However, within our numerical precision we do not observe an effect of the strip width on the propagation velocity, although we clearly observe the modification of the strain field *ahead* of the crack tip due to its advance, indicating that there are elastic disturbances that travel faster than the crack itself.

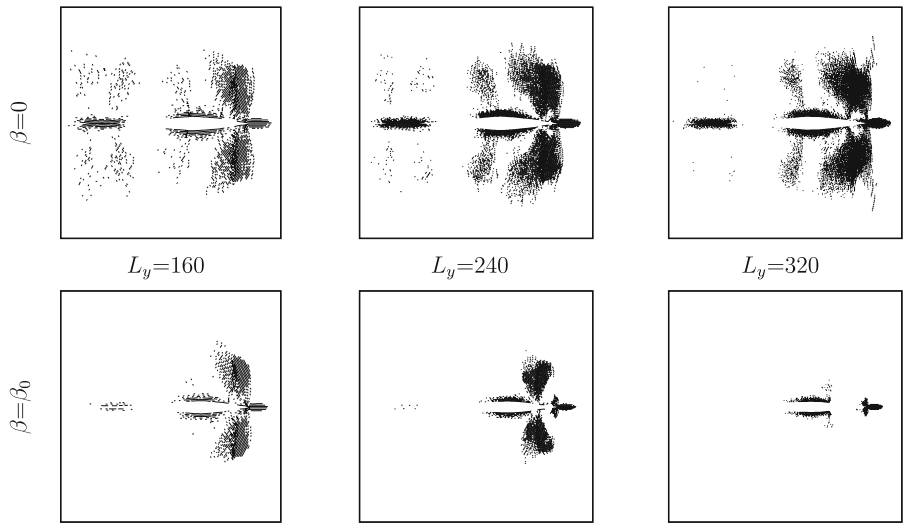

Fig. 20 Snapshots of systems of different sizes (we plot the full size in the y direction, and half the simulated system in the x direction), where only springs that are stretched beyond $u_{\rm nl}$ are shown. We see that in the absence of dissipation (*first row*) the size of the hyperelastic regions scale with the system size, whereas a fixed degree of Stokes dissipation (*second row*) makes the size of the hyperelastic region saturate when system size is increased (see also next figure). The unit used to measure dissipation is $\beta_0 = 10^{-3}\sqrt{k/m}$

The similarity of these results with those we had obtained for Mode III makes plausible that a simple explanation (such as the one found for Mode III) exists for the law that velocity depends only on $\delta/u_{\rm nl}$ also in the present case. However, we have not yet found it.

An interesting quantity to measure in the simulations with $\gamma > 1$ is the size of the hyperelastic region that drives supersonic propagation. In the super Rayleigh regime in the absence of dissipation we find (Figs. 20, 21) that the size of the hyperelastic region is proportional to the width of the strip. This result can be readily justified by a simple scaling argument in the continuum limit if independence of velocity from L_y is assumed.

In fact, suppose we have a system of width L_y in which a crack of velocity V is propagating, and suppose $\mathbf{u}_w(x, y)$ is a solution for the macroscopic displacement field in a reference system moving with the crack. Then one can immediately verify that the scaled solution $\mathbf{U}_W(x, y) \equiv \lambda \mathbf{u}_w\left(\frac{x}{\lambda}, \frac{y}{\lambda}\right)$ is the solution to the problem in a system of width $L'_y = \lambda L_y$, with the same velocity, since the boundary conditions are satisfied. In addition, from the identity $\nabla \mathbf{U}_{L'_y}|_{(x,y)} = \nabla \mathbf{u}_{L_y}|_{(\frac{x}{\lambda}, \frac{y}{\lambda})}$, it can be seen that the size of the hyperelastic region for $\mathbf{U}$ also scales with the same factor λ that governs $\mathbf{u}$. This means that the size of the hyperelastic region scales linearly with system size, and that there is not a typical size of the hyperelastic region independent of the location of the boundary in the system. This is verified in our simulations, as it can be seen in the results for $\beta = 0$ in Figs. 20 and 21.

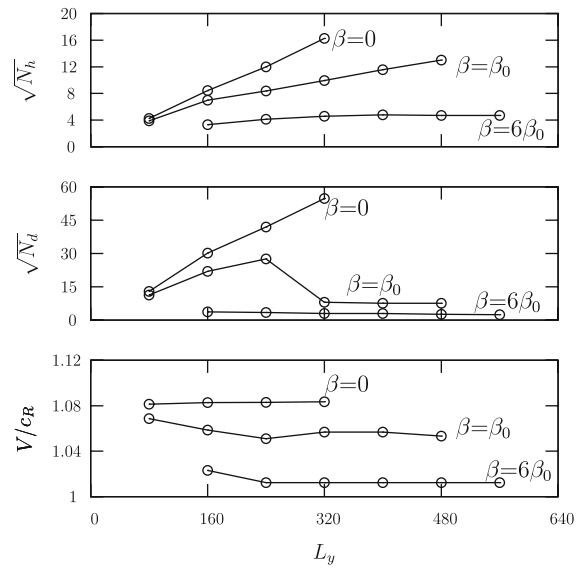

Fig. 21 Number of diagonal springs (N_d) and horizontal springs (N_h) in the nonlinear regime as a function of strip width, and crack velocities for different values of Stokes dissipation parameter β. In the absence of dissipation the linear size of the nonlinear region scales with L_y whereas for β and L_y large enough N_d collapses and N_h reaches a maximum, showing that this region remains finite. The velocity, however, does not depend strongly on β nor on L_y

The linear increase in size of the hyperelastic region with system size can however be limited by the inclusion of a finite dissipation. In Figs. 20 and 21 we see the effect of Stokes dissipation in the size of the hyperelastic region and on the velocity of the crack. The snapshots in the second row of Fig. 20 show

qualitatively that the size of the hyperelastic region does not scale with the system size in the presence of dissipation. In the more quantitative Fig. 21, we count all diagonal (N_d) and horizontal (N_h) springs that are stretched over the threshold $u_{\rm nl}$. Basically, the diagonal hyperelastic springs form the 'wings' of the 'butterfly' in Fig. 20, whereas horizontal hyperelastic springs form the small elliptical notch at the 'head' of the butterfly. The inclusion of a finite Stokes dissipation produces the disappearance of diagonal nonlinear springs when system size is increased sufficiently, and limits the size of the notch region of horizontal nonlinear springs ahead of the crack to a well defined value, independent of the system size, but dependent on the strength of the dissipation.

We see in Fig. 21 that the effect of the dissipation on the velocity is rather small, and in particular, supersonic propagation is preserved. This means that including finite dissipation, the size of the hyperelastic region can be made an arbitrarily small fraction of the total system. However, this region still drives the crack propagation supersonic. As in the mode III case, we observe that for mode I propagation, the springs that are responsible for the supersonic propagation are those lying in the crack direction, and particularly those ahead of the crack. This is clear by analyzing the situation in which dissipation is present, since in this case these are the only springs that remain in the hyperelastic regime, and propagation is still supersonic.

The results just discussed contradict the suggestion in Buehler et al. (2003), that there is a well defined relation between the size of the hyperelastic region and the crack velocity. We find in fact that this size can be set to essentially any value (by adjusting the Stokes dissipation parameter β) and yet have the crack running supersonically at the same well defined velocity. Furthermore, as we have previously shown, hyperelasticity is not necessary for the existence of supersonic motion; the size of the hyperelastic region can be zero. We conclude that neither hyperelasticity nor dissipation is critical for supersonic fracture. What is critical is that cracks remain able to propagate stably at strains that correspond to a nonzero fraction of the critical strain δ_C.

5.2 Hyperelastic softening

Although not directly related to the main theme of our paper, namely supersonic propagation, we would like to present here an interesting effect that we observe when we have hyperelastic softening ($\gamma < 1$).

Hyperelastic softening is by far the most common situation that can be expected when analyzing real materials. In fact, the simplest cohesive potential between atomic constituents of a material will generate a force that first increases linearly upon stretching, and then goes down smoothly to zero at breaking. This smooth behavior is a form of hyperelastic softening. Previous results obtained in a special model under Mode III conditions (Guozden and Jagla 2006) have shown unambiguously that softening of the springs at large deformations produces systematic reductions of the crack velocities.

The results we obtain for γ slightly below 1 are similar to those without nonlinearity ($\gamma = 0$): There is a branch where the velocity is always below the Rayleigh wave speed, and where different system sizes can be scaled by plotting them as a function of δ/δ_G (see Fig. 22), as predicted by linear elastic fracture mechanics. In addition, there are supersonic branches that are independent of system size when plotted as a function of δ/δ_C. They come into existence when $\delta/\delta_C \gtrsim .5$, as shown in Fig. 23.

For γ only slightly below 1, the velocity curve maintains a similar form to the one it had in the perfectly harmonic case, but approaching an asymptotic value for large δ/δ_G that is clearly below the Rayleigh wave speed. The saturation value of the velocity is plotted as a function of γ in Fig. 24. It can be seen that for γ close to 1, it is approximately $V \simeq c_R\sqrt{\gamma}$, which is precisely the Rayleigh velocity in a system of springs in which the spring constant has been reduced by a factor γ.

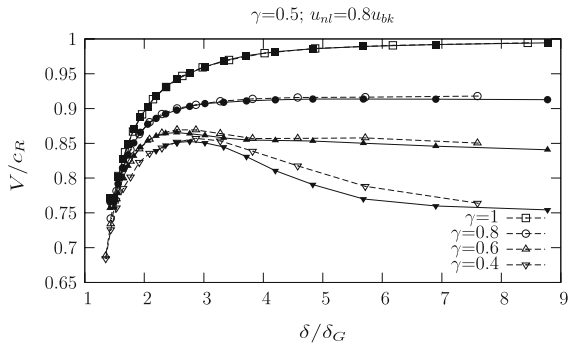

Fig. 22 Results for the velocity of a crack propagating in mode I in a system with softening nonlinearities. *Filled points* correspond to simulations with $L_y = 160$ rows, and *empty points* to $L_y = 80$ rows

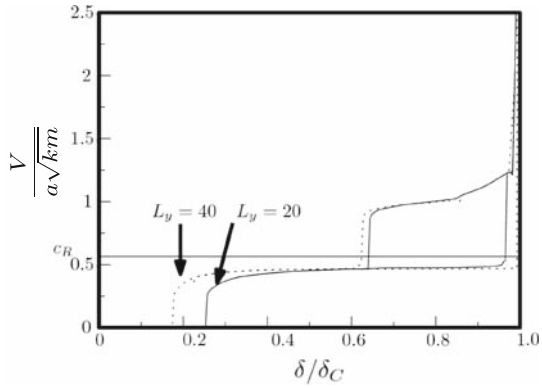

Fig. 23 Crack velocity with softening nonlinearities, scaling boundary displacement by δ_C to highlight supersonic branches. The curves are obtained from molecular dynamics. The softening parameter γ is 0.5, nonlinearity sets in at $u_{\rm nl} = (u - u_{\rm bk})/2$, and bonds break at $u_{\rm nl} = 1.015$

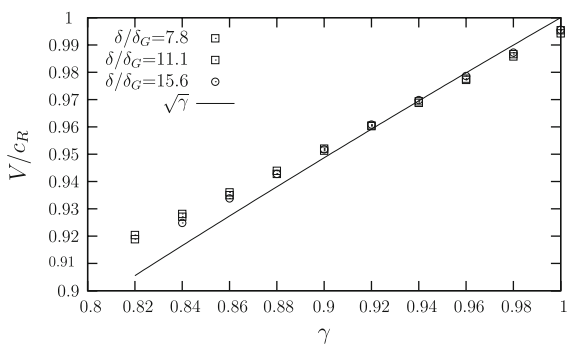

Fig. 24 Velocity at large values of $\delta/\delta_G >> 1$ as a function of the softening parameter γ. When γ is close to 1, the velocity follows approximately the law $V \sim c_R\sqrt{\gamma}$

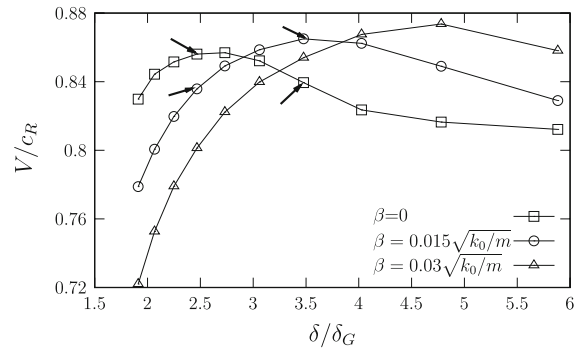

Fig. 25 Crack velocity as a function of the applied driving force, for a system with an hyperelastic constant $\gamma = 0.5$. Stokes dissipation on the system reduces the effect of decreasing velocity. Simulations pointed to with arrows are sketched in Fig. 26

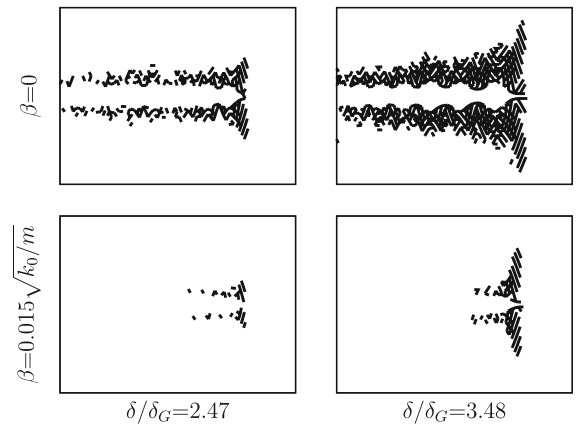

Fig. 26 Snapshots of the system from simulations corresponding to the points indicated in Fig. 25 ($\gamma = 0.5$). Only springs in the nonlinear regime are shown

If γ is sufficiently small ($\gamma < 0.6$) a qualitative change in the dependence of V on δ/δ_G is observed in Fig. 22: there is a range of applied deformation in which velocity decreases with δ. The effect is perfectly reproducible in simulations with strips of different sizes.

We emphasize that this behavior does not contradict any basic assumption of the fracture process; in particular we note that the energy consumed by crack advance continues to be an increasing function of δ. Cracks with increased driving force have been observed to slow because of side-branching (Marder and Liu 1993), but the effect here is larger, and does not involve creation of any extra surface.

Dependence of velocity on dissipation parameter in this particular regime is shown in Fig. 25. The anomalous regime in which velocity decreases with δ is destroyed by large dissipation. In addition, we see that dissipation can increase the velocity in some range of parameters.

An analysis of the hyperelastic regions in the system (Fig. 26) with and without dissipation, shows that as in the stiffening case, dissipation reduces the extent of hyperelastic regions.

A decreasing dependence of velocity on driving force may have some interesting consequences for experiments. For instance, propagation of parallel cracks with all crack tips moving exactly at the same velocity is normally impossible: even if an initial situation could be generated satisfying this configuration, any tiny acceleration of one crack with respect to the rest would produce an increase in the strain on its tip that would induce a further increase of its velocity with

respect to the others. However, in a regime of decreasing velocity with increasing driving force, an assembly of parallel cracks is stable, since a crack that travels ahead of the others receives more energy and therefore slows down. We will report in a separate publication on numerical simulations of this remarkable phenomenon.

6 Conclusions

In this work we have studied Mode I and Mode III cracks that move along weak interfaces in lattices, and have shown that they very generally admit intersonic and supersonic solutions. The range of the supersonic solution branches depends on details of the potential, the lattice geometry, and the presence of dissipation, but the supersonic states exist in all cases. The speed of the supersonic states depends upon the local stress ahead of the crack rather than energy stored per length ahead of the crack, and is not dependent upon system size.

Spring stiffening at large deformations produces the largest set of crack solutions traveling above the Rayleigh wave speed. The size of the non-linear region was studied, and we found that in the absence of dissipation this size scales as the strip width. However, in the presence of a small Stokes dissipative term, the size of the non-linear region saturates when the system size is increased sufficiently, and then for macroscopic samples the size of the non-linear region can be an arbitrarily tiny fraction of the total system size. We find no sign of a general dependence of crack velocity on the size of the non-linear region.

Spring softening at large stretching produces a decrease of the crack velocity. When the softening of the spring is large enough we found a novel regime in which crack velocity is a decreasing function of applied strain. This behavior could give rise to interesting observable consequences such as stable propagation of several cracks running parallel to one another.

Acknowledgments The authors acknowledge financial support by CONICET (Argentina) and the United States National Science Foundation (DMR0701373). Part of this work was done under grant PICT 32859/2005 (ANPCyT, Argentina).

References

Abraham FF, Gao H (2000) How fast can cracks propagate. Phys Rev Let 84:3113–3117

Andrews DJ (1976) Rupture velocity of plane-strain shear cracks. J Geophys Res 81:5679–5687

Broberg KB (1999) Cracks and fracture. Academic Press, San Diego

Buehler MJ, Gao H (2006) Dynamic fracture instabilities due to local hyperelasticity at crack tips. Nature 439:307–310

Buehler MJ, Abraham FF, Gao H (2003) Hyperelasticity governs dynamic fracture at a critical length scale. Nature 426:141–146

Burridge R, Conn G, Freund LB (1979) The stability of a rapid Mode II shear crack with finite cohesive traction. J Geophys Res 85:2210–2222

Field FA, Baker BR (1961) Crack propagation under shear displacements. J App Mech 29:436–437

Fineberg J, Marder M (1999) Instability in dynamic fracture. Phys Rep 313:1–108

Freund LB (1990) Dynamic fracture mechanics. Cambridge University Press, Cambridge

Guozden TM, Jagla EA (2005) Supersonic crack propagation in a class of lattice Models of Mode III brittle fracture. Phys Rev Let 95:224302/1–224302/4

Guozden TM, Jagla EA (2006) Some analyatical results for the velocity of cracks propagating in nonlinear lattices. Phys Rev E 74:016106/1–016106/8

Kessler DA (1999) Steady-state cracks in viscoelastic lattice models. Phys Rev E 59(5):5154–5164

Kessler DA (2000) Steady-state crakcs in viscoelastic lattice models II. Phys Rev E 61:2348–2360

Kulakhmetova SA, Saraikin VA, Slepyan LI (1984) Plane problem of a crack in a lattice. Mech Solids 19:102–108

Marder M (2004) Effect of atoms on brittle fracture. Int J Fract 130:517–555

Marder M (2005) Shock-wave theory of rupture of rubber. Phys Rev Let 94:048001/1–048001/4

Marder M (2006) Supersonic rupture of rubber. J Mech Phys Solids 54:491–532

Marder M, Gross S (1995) Origin of crack tip instabilities. J Mech Phys Solids 43:1–48

Marder M, Liu X (1993) Instability in lattice fracture. Phys Rev Let 71:2417–2420

Mott N (1947) Brittle fracture in mild steel plates. Engineering 165:16–18

Nilsson F (1972) Dynamic stress-intensity factors for finite strip problems. Int J Fract Mech 8(4):403–411. (correction, Dec 73, pp 477)

Noble B (1958) Methods based on the Wiener–Hopf technique for the solution of partial differential equations. Pergamon, New York

Petersan PJ, Deegan RD, Marder M, Swinney HL (2004) Cracks in rubber under tension exceed the shear wave speed. Phys Rev Let 93,015504/1–4

Rosakis AJ (2002) Intersonic shear cracks and fault ruptures. Adv Phys 51:1189–1257

Rosakis AJ, Samudrala O, Coker D (1999) Cracks faster than shear wave speed. Science 284:1337–1340

Schardin H (1959) Velocity effects in fracture. In: Averbach BL (ed) Fracture. MIT Press, Cambridge, MA pp 297–330

Schardin H, Mucke L, Struth W, Rhein Wa (1955) Cracking velocity of glasses. Glass Ind 36(3):133–138

Sharon E, Fineberg J (1999) Confirming the continuum theory of dynamic brittle fracture for fast cracks. Nature 397:333–335

Slepyan LI (2002) Models and phenomena in fracture mechanics. Springer, Berlin

Slepyan LI, Fishkov AL (1981) The problem of the propagation of a cut at transonic velocity. Doklady Akademii Nauk SSSR 26:1192–1193